ADVANCED FUNCTIONAL MATERIALS
www.afm-journal.de

Antimicrobial Peptide Coating of TiO_2 Nanoparticles for Boosted Antimicrobial Effects

*Lucrezia Caselli, Tanja Traini, Samantha Micciulla, Federica Sebastiani, Sebastian Köhler, Emilie Marie Nielsen, Ragna Guldsmed Diedrichsen, Maximilian W. A. Skoda, and Martin Malmsten**

This study explores the coating of photocatalytic nanoparticles with antimicrobial peptides (AMPs) for boosted antimicrobial effects, and how such effects depend on AMP properties. For this, TiO_2 nanoparticles are coated with the AMP KYE21 or its hydrophobically enhanced variant WWWKYE21. Mirroring effects of free peptides, coated nanoparticles displayed higher binding and UV-induced degradation for bacteria-like than for mammalian-like membranes. In addition, they degraded bacterial lipopolysaccharides (LPS). WWWKYE21-coated nanoparticles displayed higher binding to LPS and bacteria-like membranes and photocatalytic degradation, although saturation effects are found at high nanoparticle binding. Neutron reflectometry showed that binding of peptide-coated nanoparticles to bacteria-like membranes resulted in partial lipid removal in the absence of UV, but that UV illumination caused additional degradation, featuring increases in the hydration of headgroup and acyl chain regions. For LPS, UV induced removal of its outer O-antigen region. Analogous to findings in model systems, antimicrobial effects of peptide-coated nanoparticles against Escherichia coli bacteria on illumination are pronounced, while toxicity against human monocytes remained low. Altogether, results show that AMP coating boosts the antimicrobial effects of photocatalytic nanoparticles without causing cell toxicity. From a broader perspective, the study points to the potential of nanoarchitectonic combination of component properties for the design of composite NP properties.

1. Introduction

Photocatalytic nanoparticles are promising systems in the fight against bacterial infections, as they may be designed to potently suppress a wide spectrum of bacteria in both planktonic and biofilm states, including strains resistant to conventional antibiotics.[1–4] Antimicrobial effects of photocatalytic nanoparticles are related to the generation of free electrons and holes under illumination, which react with water and dissolved oxygen (as well as other solutes) to form reactive oxygen species (ROS) such as $\cdot O_2^-$ and ·OH. The latter are highly reactive, able to degrade essential bacterial components such as membrane lipids and lipopolysaccharides, as well as enzymes and DNA. Demonstrating the potency of photocatalytic nanomaterials, Sułek et al. reported porphyrin-doped TiO_2 nanoparticles to result in a 7-log reduction of *Staphylococcus aureus* under illumination,[5] while Ahmed et al. reported potent antimicrobial effects of TiO_2 nanoparticles on 25 multi-drug resistant *Pseudomonas aeruginosa* strains.[6] The development of photocatalytic nanomaterials toward therapeutics is, however, precluded by poor selectivity between bacteria and human cells.[1] Considering this approaches for targeting photocatalytic nanoparticles to bacteria may potentially increase their antimicrobial potency without simultaneously increasing their toxicity. Exploring this approach, we recently reported on photocatalytic TiO_2 nanoparticles coated with the antimicrobial peptide (AMP) LL-37 (LLGDFFRKSKEKIGKEFKRIVQRIKDFLRNLVPRTES).[7] The peptide-coating was found not to significantly suppress ROS

L. Caselli, F. Sebastiani, M. Malmsten
Department of Physical Chemistry
Lund University
Lund SE-22100, Sweden
E-mail: martin.malmsten@sund.ku.dk

The ORCID identification number(s) for the author(s) of this article can be found under https://doi.org/10.1002/adfm.202405047

DOI: 10.1002/adfm.202405047

T. Traini, F. Sebastiani, E. M. Nielsen, R. G. Diedrichsen, M. Malmsten
Department of Pharmacy
University of Copenhagen
Copenhagen DK-2100, Denmark

S. Micciulla
Institut Laue–Langevin
CS 20156, Grenoble 38042 Cedex 9, France

S. Köhler
LINXS Institute for Advanced Neutron and X-ray Science
Scheelevagen 19, Lund 22370, Sweden

M. W. A. Skoda
ISIS Pulsed Neutron and Muon Source
Rutherford Appleton Laboratory
Harwell OX11 0QX, UK

formation by TiO_2 nanoparticles, and to be sufficiently stable to allow enhanced binding to bacteria-like phospholipid membranes, as well as strongly boosted degradation of these under UV illumination. In contrast, oxidative degradation of mammalian-like cholesterol-containing membranes was much lower.

While this recent study demonstrated the potential of AMP-coating photocatalytic nanoparticles for boosted antimicrobial effects, it remains unclear to what extent molecular AMP properties translate to AMP-coated nanoparticles. This is an important aspect since various approaches have been previously identified in the literature to design AMPs displaying potent antimicrobial effects and simultaneously low toxicity.[8,9] In addition, extensive literature exists on how molecular properties of AMPs in solution can be employed to control their interaction with bacterial membranes and lipopolysaccharides.[10–12] This previous literature thus represents a potential source of systems that can be used for AMP-coated photocatalytic nanoparticles. However, since AMPs will likely rely on similar molecular properties for membrane interactions and binding to photocatalytic nanoparticles, it is unclear to what extent molecular AMP properties in solution are relevant for AMP-coated nanoparticles. For example, hydrophobic and positively charged amino acids, which are key for bacterial membrane destabilization for free AMPs,[8–11] may be needed for nanoparticle binding, thereby becoming unavailable for membrane interactions of peptide-coated nanoparticles. Similarly, amphiphilic helix formation, key for some AMPs, may be hindered by the AMP being immobilized at the nanoparticle surface.

In this study, we investigate the effects of linear amphiphilicity using the AMPs KYE21 (KYEITTIHNLFRKLTHRLFRR) and WWWKYE21, the latter displaying higher amphiphilicity due to end-tagging with hydrophobic tryptophan residues. Such W-tagging has previously been found to promote binding to bacterial lipid membranes and LPS, resulting in strongly boosted antimicrobial and anti-inflammatory effects.[13] A key feature of the W-tag is that this strongly promotes peptide binding, insertion, and destabilization of anionic and cholesterol-void bacteria membranes.[14–17] For mammalian membranes, which are dominated by zwitterionic phospholipids and contain a sizeable fraction of cholesterol,[18,19] however, peptide insertion is energetically costly.[20,21] As a result of this, WWWKYE21 and other W-tagged peptides display modest binding to, and destabilization of, mammalian membranes. Together, these features provide W-tagged peptides with potent antimicrobial/anti-inflammatory effects at simultaneously low toxicity against human cells.

Based on this, we here investigated the effects of W-tagging on the performance of *AMP-coated* TiO_2 nanoparticles. The latter were chosen due to their wide bandgap (3.4 eV[22]), which requires UV for ROS generation and thus allows effects of direct particle effects ("in darkness") to be distinguished from effects of ROS formation under UV illumination. For these systems, we investigated: i) the effects of peptide coating on nanoparticle colloidal stability, ii) the effect of the peptide coating on ROS generation, and iii) the robustness of the peptide coating to oxidative degradation (**Figure 1**). Having demonstrated advantageous effects here, we employed quartz-crystal microbalance with dissipation monitoring (QCM-d) to show that peptide-coating of TiO_2 nanoparticles results in increased binding to bacteria-like phospholipid membranes and LPS, as well as in boosted degradation under UV illumination under conditions relevant to skin and wound infections[23] (Figure 1). Furthermore, structural variations associated with membrane oxidative degradation were investigated by neutron reflectometry. Finally, the relevance of such model systems for antimicrobial effects and cell toxicity was demonstrated (Figure 1).

2. Result

2.1. Peptide Coating of TiO_2 Nanoparticles

In its anatase form, TiO_2 has an isoelectric point of ≈6–6.5,[24,25] which means that it carries a low net negative charge at physiological pH. KYE21 and WWWKYE21, on the other hand, both have an isoelectric point of 11.7 and carry a net positive charge at pH 7.4. Together with the presence of hydrophobic residues in these peptides, this causes peptide binding to the TiO_2 nanoparticles. Demonstrating this, the ζ-potential of TiO_2 nanoparticles at pH 7.4 displayed a buildup of an increasingly positive ζ-potential with increasing peptide concentration. For both peptides, a strongly positive ζ-potential was observed after loading 100 ppm of TiO_2 nanoparticles from 50 μM peptide solution, corresponding to 40 ± 2 mV for KYE21 and 35 ± 2 mV for WWWKYE21 (**Figure 2A**). Mirroring the ζ-potential results, particle size measurements showed bare TiO_2 nanoparticles to be colloidally unstable at pH 7.4 due to their low surface charge. Upon peptide loading, the positive surface charge build-up suppresses nanoparticle aggregation, resulting in well-dispersed peptide-coated TiO_2 nanoparticles. WWWKYE21 was found to be more efficient in providing colloidal stability to the TiO_2 dispersion than KYE21, seen by WWWKYE21 requiring a lower peptide concentration (30 μM) to reach well-dispersed TiO_2 nanoparticles, whereas a peptide concentration of 50–70 μM is needed for KYE21 (Figure 2A). Peptide-mediated stabilization of TiO_2 NPs was found also for 10 mM acetate, pH 5.4 (Figure S1, Supporting Information).

2.2. UV-Induced Degradation of Peptide Coatings

While providing beneficial colloidal stabilization of TiO_2 nanoparticles, peptides are susceptible to photocatalytic degradation.[26,27] Hence, there is a risk that the peptide coatings are oxidatively degraded upon UV illumination. Looking into the kinetics for this, we investigated how the ζ-potential of the peptide-coated TiO_2 nanoparticles depended on UV exposure. As shown in Figure 2B, the ζ-potential decreased slightly with increasing UV exposure time for both KYE21 and WWWKYE21, indicating oxidation and/or oxidative cleavage. Importantly, however, the peptide-loaded nanoparticles remained positively charged also after 2 h of UV illumination, indicating that while UV exposure caused some peptide oxidation and likely degradation, this is incomplete after 2 h of UV exposure. A similar behavior was also observed at pH 5.4 (Figure S2, Supporting Information). These results show that both the KYE21 and WWWKYE21 coatings are sufficiently resilient to UV-induced oxidation to allow peptide-loaded TiO_2 nanoparticles to be employed in subsequent experiments with QCM-d, neutron reflectometry, and biological assays.

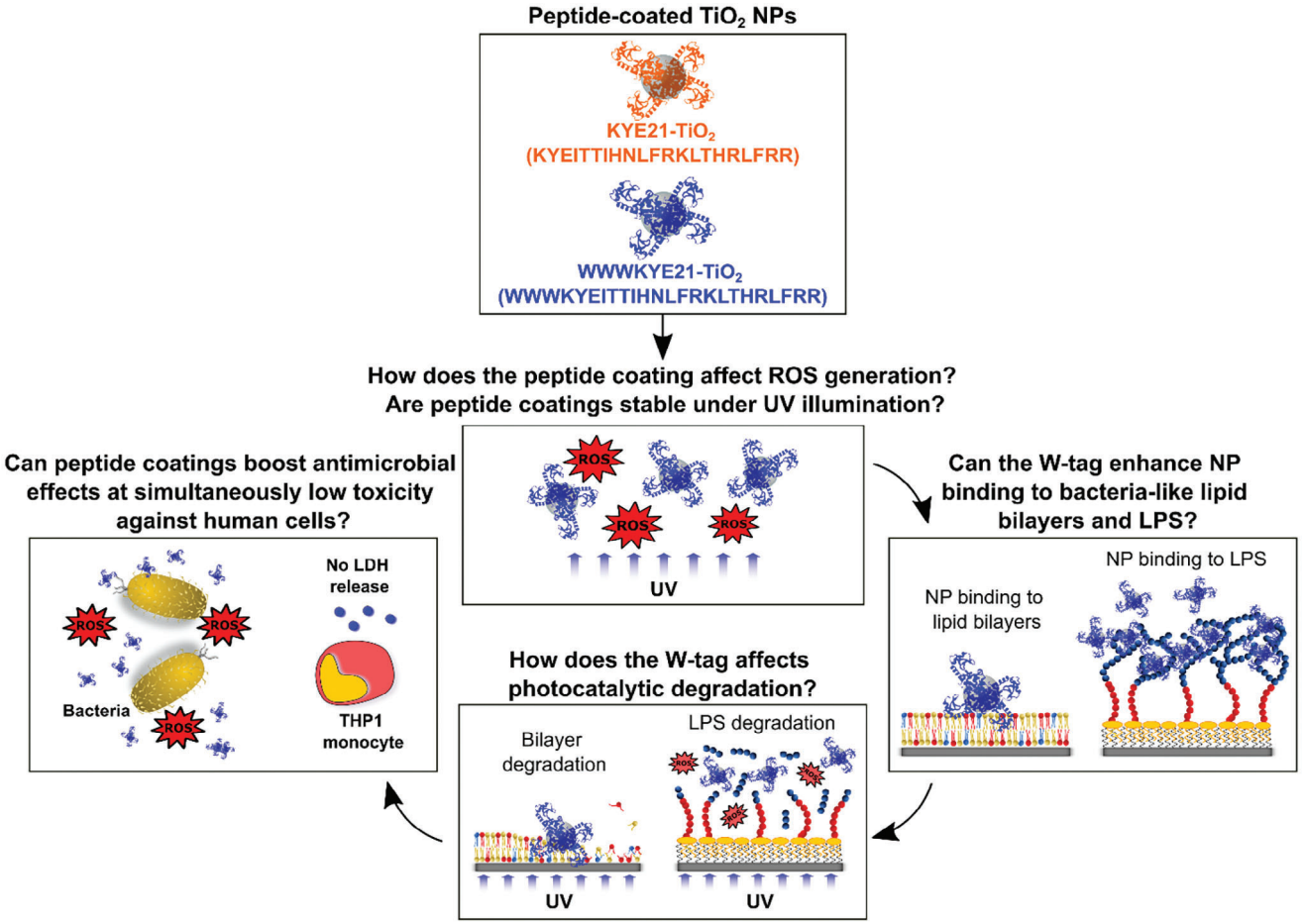

Figure 1. Schematic illustration describing the approach taken and the research questions addressed: i) TiO_2 NPs coated with the peptides KYE21 and WWWKYE21 were prepared and characterized regarding colloidal stability and ROS generation; ii) subsequently, binding of peptide-coated TiO_2 NPs to bacteria-like bilayers and LPS, as well as photocatalytic degradation under UV illumination was assessed; iii) finally, antimicrobial effects and cell toxicity of peptide-coated particles were investigated.

2.3. UV-Induced ROS Generation

Since ROS formation requires photogenerated electrons and holes in the TiO_2 nanoparticles to react with ambient water, dissolved oxygen, or solutes, there is a risk that the surface coatings suppress ROS generation. Addressing this, we investigated ROS generation by C_{11}-BODIPY assay. As seen in Figure 2C, Figures S3 and S4 (Supporting Information), both KYE21-TiO_2 and WWWKYE21-TiO_2 displayed pronounced ROS generation on UV illumination. Quantitively, results are comparable to those that we previously found for bare TiO_2 NPs in the same pH range[7] or at pH 3.4[28] (summarized in Figure S5, Supporting Information). Together, this suggests that the peptide coatings do not dramatically suppress the ROS generation of the TiO_2 nanoparticles.

2.4. UV-Induced Degradation of Phospholipid Membranes

To monitor the oxidative degradation of phospholipid membranes further, we employed QCM-d. To this purpose, lipid bilayers were formed onto silica substrates, resulting in well-defined +PG, PC, and +Chol bilayers.[28] To such bilayers, peptide-coated TiO_2 nanoparticles were added, monitoring nanoparticle binding in terms of frequency shift and dissipation. As can be seen in **Figure 3**A, Figures S6A and S7A (Supporting Information), the binding of both KYE21-TiO_2 and WWWKYE21-TiO_2 at pH 7.4 was significantly higher to anionic +PG bilayers than to zwitterionic PC and +Chol bilayers. For both KYE21-TiO_2 and WWWKYE21-TiO_2, binding to +PG was much higher than that of bare TiO_2 nanoparticles (Figure 3B; Figure S8A, Supporting Information). Mirroring this, UV-induced oxidative degradation caused more pronounced membrane destabilization for +PG than for PC and +Chol (Figure 3C; Figure S6B and S7B, Supporting Information). Importantly, both peptide-coated NPs induced a dramatically higher removal of bacteria-like +PG bilayer (Figure 3D; Figure S8B, Supporting Information), compared to bare TiO_2 NPs. Similar results, both in terms of membrane binding and oxidative degradation, were observed at pH 5.4 (Figure S9, Supporting Information). It was furthermore confirmed that removing unsaturated PAPC from the lipid bilayer composition (added to enhance UV irradiation efficiency at larger

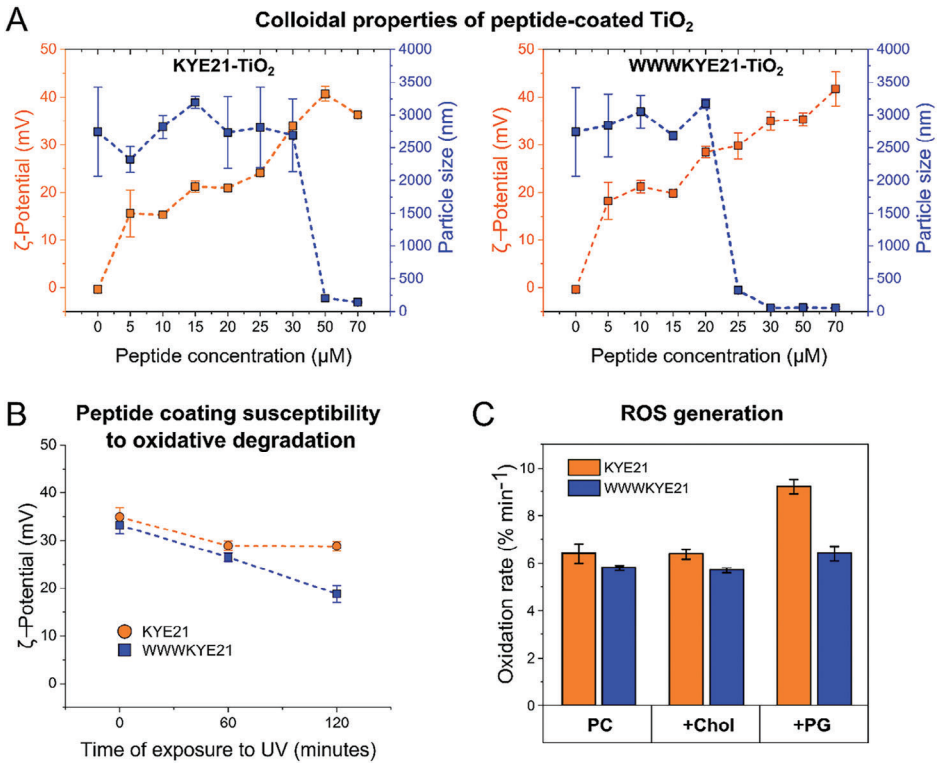

Figure 2. Characterization of peptide-coated TiO_2 NPs. A) ζ-potential and average particle size of TiO_2 nanoparticles (100 ppm) loaded at varying concentrations of either KYE21 (left) or WWWKYE21 (right) in 10 mM Tris, pH 7.4. ($n = 3$). Corresponding results obtained in 10 mM acetate, pH 5.4, are shown in Figure S1 (Supporting Information). B) ζ-potential of TiO_2 nanoparticles coated with 50 μM KYE21 or WWWKYE21 in 10 mM Tris, pH 7.4, before and after 1 or 2 h of UV illumination. ($n = 3$). Corresponding results obtained in 10 mM acetate, pH 5.4, are shown in Figure S2 (Supporting Information). C) C_{11}-BODIPY oxidation rates for KYE21- or WWWKYE21-coated TiO_2 nanoparticles on PC, +Chol, and +PG LUVs subjected to in situ UV exposure in 10 mM Tris, pH 7.4. ($n = 3$). Corresponding oxidation kinetics are shown in Figure S3 (Supporting Information), while results in 10 mM acetate, pH 5.4, are shown in Figure S4 (Supporting Information).

sample/UV-lamp distances, which conveniently reduces the risk of sample heating in the case of bare TiO_2 nanoparticles) did not substantially influence UV-induced degradation of +PG, PC and +Chol bilayers (Figure S10, Supporting Information).

2.5. UV-Induced Degradation of Bacterial Lipopolysaccharides

Having investigated the photocatalytic degradation of bacteria-like and mammalian-like phospholipid membranes, we next employed the same methodology for surface-bound LPS. For this, either smooth or rough *E. coli* LPS (the latter characterized by having longer hydrophilic polysaccharide chains[29,30]) were first adsorbed to hydrophobic silica slides (pre-coated with OTS) through their hydrophobic lipid A moiety, thus in the same orientation as when bound to bacteria membranes. For comparison, the lipid A moiety alone was immobilized as well. As shown in Figure S11 (Supporting Information), LPS bound to a significant amount on the hydrophobic surfaces, reaching a saturation frequency shift -26 ± 3 and -61 ± 5 Hz for smooth and rough LPS, respectively, and -25 ± 5 Hz for lipid A. In addition to KYE21-TiO_2 or WWWKYE21-TiO_2 to such layers after removal of remaining free LPS from solution, substantial nanoparticle binding was observed for both LPS and lipid A (**Figure** 4A; Figure S12A and S13A, Supporting Information). Quantitatively, the binding of KYE21-TiO_2 or WWWKYE21-TiO_2 was comparable for smooth LPS and lipid A, as seen from frequency shifts up to −10 Hz. Rough LPS displayed an even higher binding for both peptides and especially so for WWWKYE21-TiO_2 NPs ($\Delta F = -115 \pm 9$, compared to $\Delta F = -25 \pm 3$ for KYE21-TiO_2 NPs. In contrast, very little absorption of bare TiO_2 NPs was detected on either smooth or rough LPS layers (Figure 4B; Figure S14A, Supporting Information). On UV illumination, a positive frequency change was observed for LPS and lipid A incubated with peptide-coated TiO_2 NPs, reporting on oxidative degradation (Figure 4C; Figure S12B, and S13B, Supporting Information). In line with the results on binding, the highest nanoparticle-induced degradation was observed for rough LPS (corresponding to $\Delta F = +51 \pm 7$ Hz for WWWKYE21-TiO_2 and $+12 \pm 3$ Hz for KYE21-TiO_2). Furthermore, mirroring the results on binding, bare TiO_2 NPs were significantly less effective than WWWKYE21-TiO_2 NPs inducing oxidative LPS degradation (Figure 4D; Figure S14B, Supporting Information).

2.6. Structural Aspects of Lipid Membrane Degradation

To obtain structural information on UV-induced degradation, neutron reflectometry was employed for WWWKYE21-TiO_2 NPs interacting with +PG bilayers. For this, experiments were

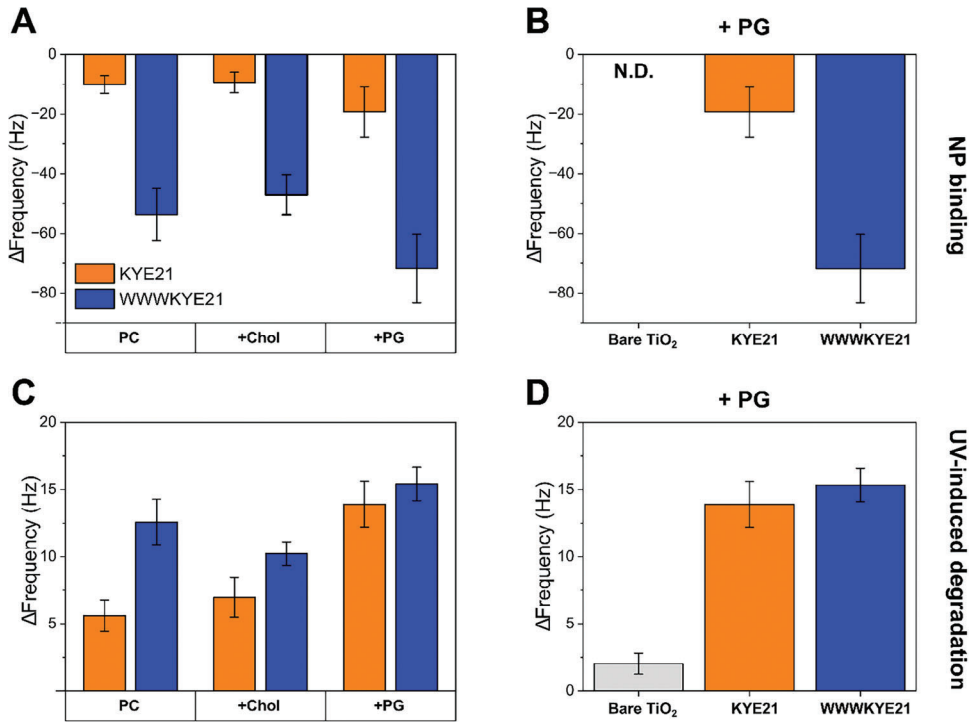

Figure 3. QCM-d results showing frequency shifts caused by: A) binding of 20 ppm of KYE21-TiO_2 and WWWKYE21-TiO_2 to PC, +Chol and +PG bilayers; B) binding of 20 ppm bare TiO_2, KYE21-TiO_2 and WWWKYE21-TiO_2 to +PG bilayers; C) effects of 2 h of in situ UV illumination for PC, +Chol and +PG interacting with 20 ppm KYE21-TiO_2 and WWWKYE21-TiO_2; D) effects of 2 h of in situ UV illumination for +PG incubated with 20 ppm bare TiO_2, KYE21-TiO_2 and WWWKYE21-TiO_2. $\Delta F = 0$ corresponds to the Frequency shift for the lipid bilayer right before NP binding (A and B) or UV illumination (C and D). All measurements were performed in 10 mM Tris, pH 7.4. ($n = 3$). Representative QCM-d profiles are shown in Figure S6 (Supporting Information) (for KYE21-loaded TiO_2 NPs), S7 (for WWWKYE21-loaded TiO_2 NPs), and S8 (Supporting Information) (for bare TiO_2 NPs). Corresponding results obtained in 10 mM acetate, pH 5.4, are shown in Figure S9 (Supporting Information).

performed in 10 mM Tris buffer at pH 7.4, prepared in H_2O (h-Tris), 68.6/31.4% v/v D_2O/H_2O mixture (qm-Tris, with SLD matching the one of quartz), and D_2O (d-Tris). Results obtained in the three contrasts were fitted simultaneously to a four-layer model (Scheme S1, Supporting Information), with input parameters summarized in Tables S1 and S2 (Supporting Information). To reduce the number of free parameters, the head group thickness was fixed at 7.5 Å.[31] Prior to NP addition, +PG bilayers presented >99% coverages and low (≈0%) tail hydration (Table S2, Supporting Information). Values of area per molecule (APM), headgroups hydration, bilayer thickness, and surface coverage (Γ) were calculated as described previously[28] and are consistent with previous literature[32,33] (Table S2, Supporting Information). Shown in Figure S15 (Supporting Information) are reflectivity profiles with best curve fits and corresponding SLD for the +PG bilayer interacting with 20 ppm WWWKYE21-TiO_2 NPs, before and after 2 h of UV illumination. Reflectivity data and corresponding SLD profiles of the bilayer prior to NP addition are included for comparison. Key structural data obtained from neutron reflectometry fits are plotted in **Figure 5** and listed in full in Table S2 (Supporting Information). Already in the absence of UV illumination, significant structural modification of +PG was detected upon incubation with WWWKYE21-TiO_2 NPs. Specifically, a concomitant increase in the hydration of polar headgroups and acyl chains of the lipid bilayer was observed, leading to an overall increase of the APM from 70 ± 4 to 98 ± 5 $Å^2$. In parallel, the thickness of the bilayer decreased from 47.4 ± 0.8 Å before nanoparticle addition to 37.6 ± 0.8 Å after the addition of WWWKYE21-TiO_2 NPs, accompanied by a significant lipid removal (Γ decreasing from 3.6 ± 0.1 mg m^{-2} to 2.6 ± 0.2 mg m^{-2}). Upon UV illumination, additional membrane destabilization was observed, leading to a final APM of 121 ± 6 $Å^2$, a surface coverage of 2.0 ± 0.1 mg m^{-2}, and increases in the hydration of the polar headgroup (58 ± 6%) and acyl chain regions (9 ± 4%), respectively.

2.7. Structural Aspects of Lipopolysaccharide Degradation

To obtain information on structural features of UV-induced LPS degradation, neutron reflectometry was employed for 20 ppm WWWKYE21-TiO_2 interacting with smooth LPS. The effect of bare TiO_2 was also investigated for comparison. Experiments were performed in 10 mM h-, qm- and d-Tris buffers, pH 7.4, containing 150 mM NaCl (the higher ionic strength needed for dense LPS layer formation). For this, quartz blocks were pre-functionalized with OTS,[34,35] forming a homogeneous hydrophobic layer exposed to the water solution. Such layer was characterized in three contrasts before the injection of LPS (Figure S16, Supporting Information). Structural parameters describing the OTS layer (Table S3, Supporting Information), obtained from NR fits, were consistent with previous literature.[34,35]

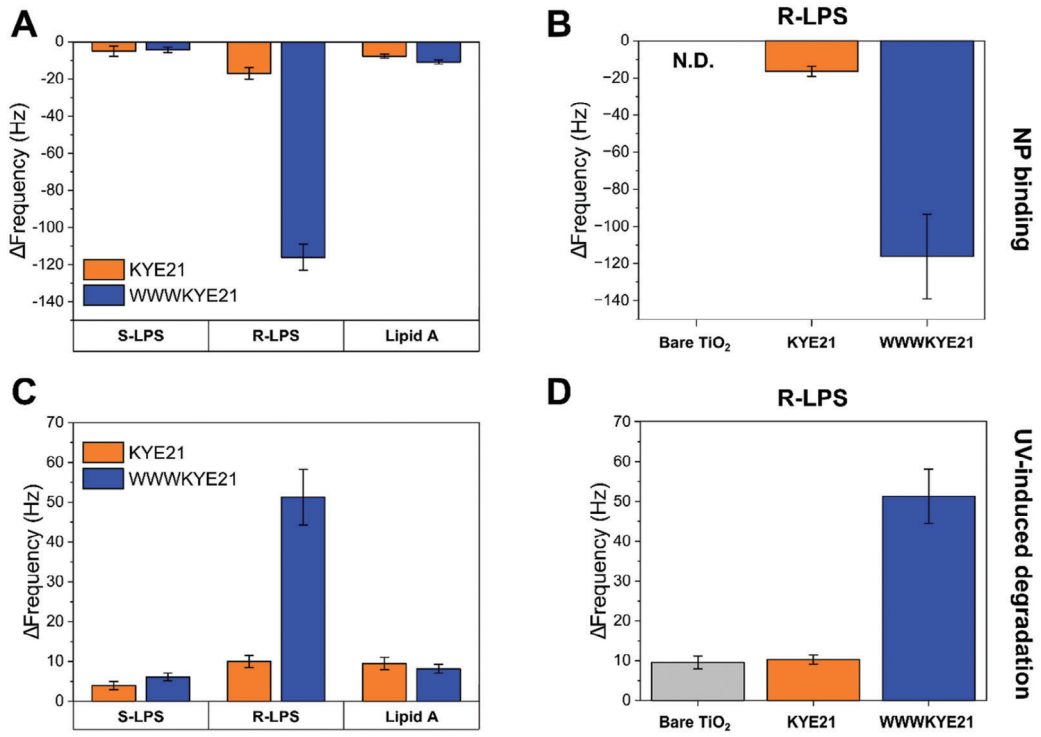

Figure 4. QCM-d results showing frequency shifts caused by A) binding of 20 ppm KYE21-TiO_2 and WWWKYE21-TiO_2 to smooth LPS (S-LPS), rough LPS (R-LPS) and lipid A; B) binding of 20 ppm bare TiO_2, KYE21-TiO_2, and WWWKYE21-TiO_2 to rough LPS; C) effects of 2 h of in situ UV illumination for smooth LPS, rough LPS and lipid A interacting with 20 ppm KYE21-TiO_2 and WWWKYE21-TiO_2; D) effects of 2 h of in situ UV illumination on rough LPS incubated with 20 ppm bare TiO_2, KYE21-TiO_2 and WWWKYE21-TiO_2. $\Delta F = 0$ corresponds to the Frequency shift for smooth LPS, rough LPS, and lipid A layers right before NP binding (A and B) or UV illumination (C and D). All measurements were performed in 10 mM Tris + NaCl 150 mM, pH 7.4. Representative QCM-d profiles for Figure (A) and (B) are shown in Figure S12 (Supporting Information) (for KYE21-TiO_2 NPs), Figure S13 (Supporting Information) (for WWWKYE21-TiO_2 NPs), and Figure S14 (Supporting Information) (for bare TiO_2 NPs). ($n = 3$).

The LPS layer was subsequently formed by direct injection into the liquid-solid flow cell and the reflectivity was acquired. NR profiles obtained in three different contrasts (Figure S17, Supporting Information for bare TiO_2 NPs and Figure S18, Supporting Information for WWWKYE21-TiO_2 NPs) were fitted simultaneously to a three-layer model (Scheme S2, Supporting Information), featuring: i) an internal hydrophobic layer of lipid A fully interdigitated with OTS; ii) a second layer containing the core oligosaccharide moiety of smooth LPS, and iii) an outer layer of O-antigen chains. The SLDs of such layers were taken from previous literature[35–37] and used as input parameters for data fitting (Table S4, Supporting Information for bare TiO_2 NPs and Table S5, Supporting Information for WWWKYE21-TiO_2 NPs). Values of initial thickness, hydration, and roughness were obtained for each layer (Tables S4 and S5, Supporting Information; Figure 6) and were in line with previous reports on similar LPS systems.[35,36] Reflectivity profiles with best curve fits and corresponding SLD for smooth LPS interacting with 20 ppm WWWKYE21-TiO_2 NPs, before and after 2 h of UV illumination, are shown in Figure S18 (Supporting Information). Key structural data obtained from NR fits are listed in full in Table S5 (Supporting Information). Upon incubation with bare TiO_2 NPs and in the absence of UV illumination, no significant structural modification was detected in any of the LPS layers (Figure S17 and Table S4, Supporting Information). Similarly, WWWKYE21-TiO_2 NPs did not significantly modify the structure of the internal smooth LPS layers, i.e., the mixed OTS/Lipid A and core oligosaccharides moieties. In contrast, the outer O-antigen chains layer underwent a substantial decrease in thickness with the addition of WWWKYE21-TiO_2 NP, from 103 ± 8 to 32 ± 7 Å. UV illumination caused a further decrease in the thickness of O-antigen chains (to 12 ± 4 Å) and hydration (from 94 ± 1 to 70 ± 10%), indicating an almost complete removal of the outer O-antigen layer. In contrast, only a mild size reduction of O-antigen chains was detected upon UV illumination in the presence of bare TiO_2 NPs, i.e., from 105 ± 12 (before UV) to 84 ± 17 Å (after UV), with negligible hydration changes. For both bare and WWWKYE21-coated TiO_2 NPs, the internal layers of OTS/Lipid A and core oligosaccharides were largely unaffected by UV illumination.

2.8. Antibacterial Effects and Cell Toxicity

To investigate if results for model lipid bilayers are relevant for bacterial and human cell membranes, we next investigated antimicrobial effects and cell toxicity. In doing so, confocal microscopy was employed to study the effects of bare, WWWKYE21-coated, or KYE21-coated TiO_2 NPs on Gram-negative *E. coli* bacteria at pH 7.4 and 5.4. For this, a two-color fluorescence LIVE/DEAD assay was used, allowing differentiation between bacteria with intact cell membranes (staining green) and those

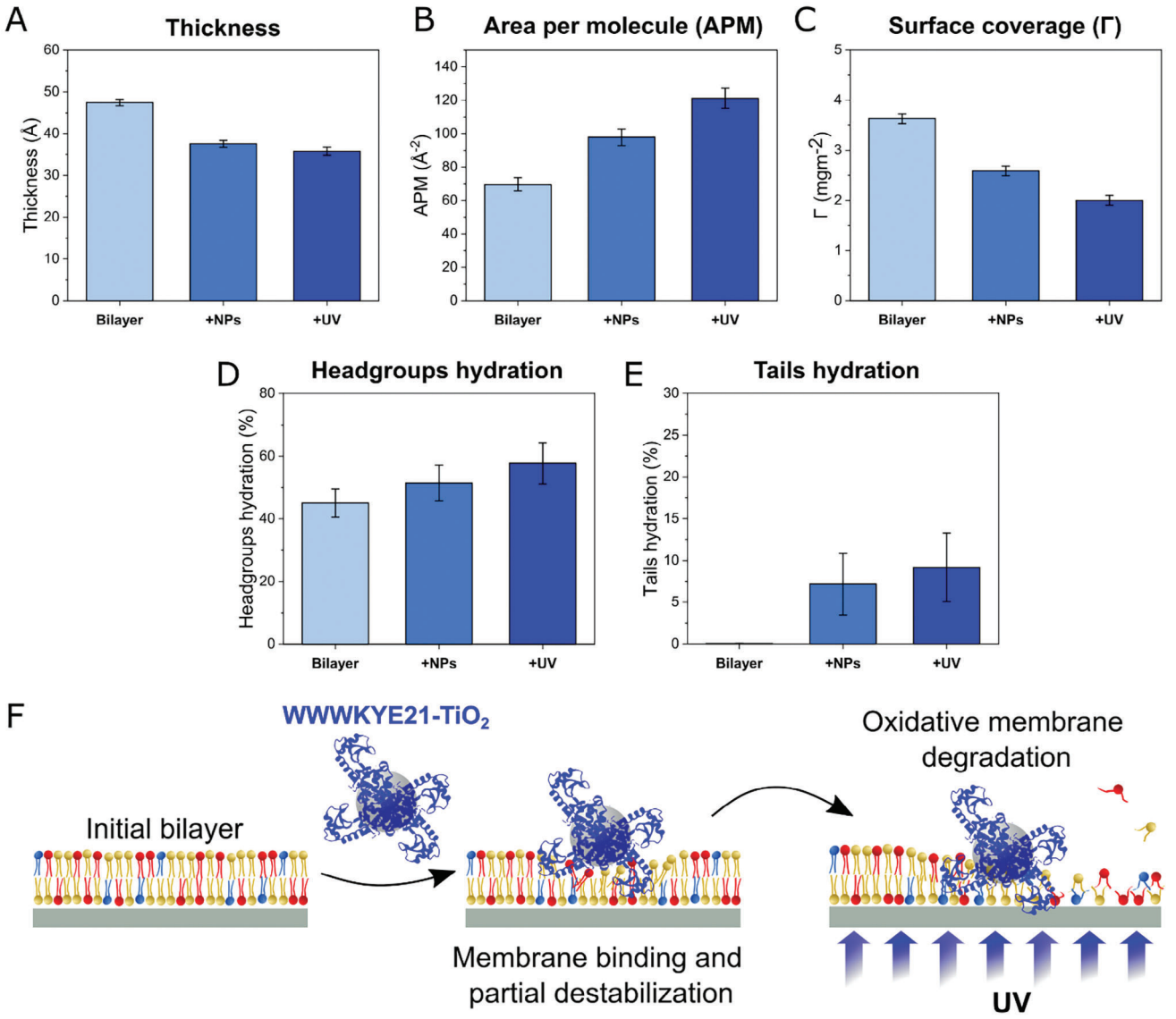

Figure 5. Structural effects on supported +PG bilayers with WWWKYE21-coated TiO_2 NPs. The reported parameters were extracted from neutron reflectometry fits for the system before nanoparticle incubation, after nanoparticle incubation, and after 2 h of in situ UV exposure. Shown are changes in (A) bilayer thickness, B) area per lipid molecule (APM), C) surface coverage of the supported lipid bilayer (Γ), D) hydration of the hydrophilic headgroups, and E) hydration of the hydrophobic tails. Shown in (F) is a schematic illustration describing the main structural changes observed for the lipid bilayer upon NPs interaction and UV illumination. Corresponding experimental curves, together with best-fit curves and calculated SLD profiles, are shown in Figure S15 (Supporting Information).

with damaged membranes (staining red). Representative confocal microscopy images acquired at pH 5.4 are shown in **Figure** 7A, while corresponding images at pH 7.4 are shown in Figure S19 (Supporting Information). Results extracted from image analysis are reported in Figure 7B,C, for pH 5.4 and 7.4, respectively. Already in the absence of UV illumination, both KYE21- and WWWKYE21-TiO_2 NPs display boosted antimicrobial activity on *E. coli* compared to bare TiO_2 NPs. For both peptides, bacteria-killing was promoted under UV illumination, especially at pH 5.4, leading to 77 ± 4% and 91 ± 4% dead *E.coli* for KYE21- and WWWKYE21-TiO_2 NPs, respectively.

The toxicity of peptide-coated nanoparticles toward eukaryotic cells was monitored by the release of the intracellular enzyme lactate dehydrogenase. For this, THP1 monocytes were exposed to bare, KYE21- and WWWKYE21-TiO_2 NPs, with or without UV illumination. Despite the strong antimicrobial effects associated with peptide-coated TiO_2 NPs, lactate dehydrogenase experiments demonstrated that both bare and KYE21- or WWWKYE21-TiO_2 NPs (either before or after UV illumination) did not induce any significant membrane rupture and resultant release of intracellular lactate dehydrogenase (**Figure** 8). Similarly, no significant increases in LPS-induced cell toxicity were observed upon

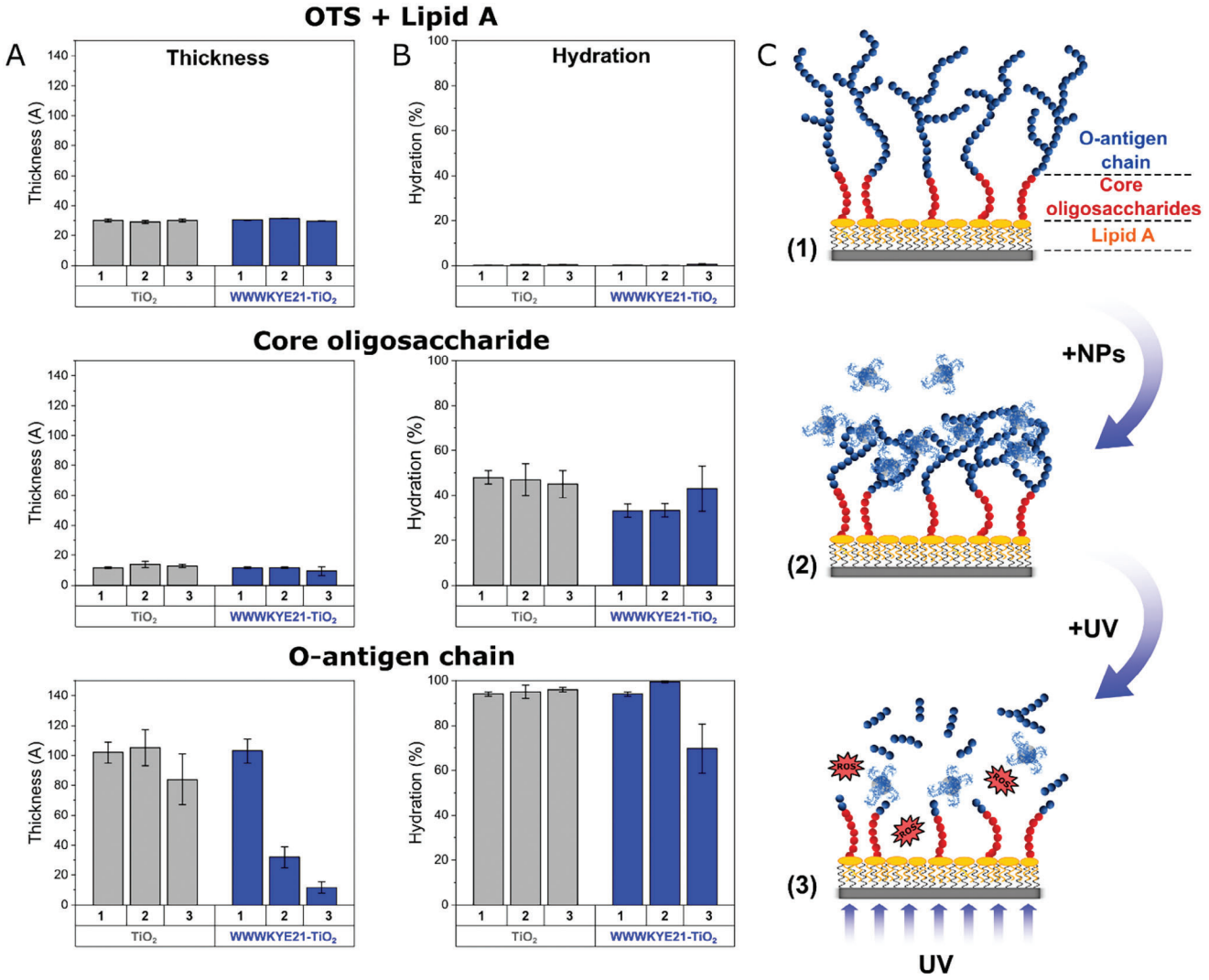

Figure 6. Structural effects on OTS + Lipid A (top), Core oligosaccharide (middle), and O-antigen chain (bottom) layers induced by bare and WWWKYE21-coated TiO_2 NPs, in the absence and presence of UV illumination. Results were obtained from neutron reflectometry fits, calculating the physical parameters of the bilayers at different time points: 1) before NP incubation; 2) after NP incubation; 3) after 2 h of in situ UV exposure. Shown are changes in the thickness A) and hydration B) for the three different layers, as well as a schematic illustration C) describing the main structural changes observed for the different LPS domains upon WWWKYE21-coated TiO_2 NPs interaction and UV illumination. Corresponding experimental curves, best curve fits, and calculated SLD profiles, are shown in Figure S17 (Supporting Information), while Figure S16 (Supporting Information) collects experimental curves, together with best curve fits and SLD profiles, for the neat OTS layer grafted before LPS.

incubation of LPS with bare and peptide-coated TiO_2 NPs, both prior to and after UV illumination.

3. Discussion

3.1. Effects of AMP Coating on NP Properties

Previous results in literature have shown that cationic surface modifications may promote nanoparticle interaction with bacterial membranes and membrane components, thereby boosting antimicrobial effects.[38] For photocatalytic nanoparticles, however, the situation is more complex than for other types of nanoparticles, since photogenerated electrons and holes must be able to react with water, dissolved oxygen, or other solutes to form ROS and trigger antimicrobial effects.[1] This means that surface modification may potentially jeopardize antimicrobial effects by preventing ROS formation, either by suppressing the transport rate of photogenerated electrons and holes through the surface layer or by reacting with the latter to form surface-bound oxidized species. As the desorption of peptides is much slower than ROS lifetime,[39,40] this may cause ROS generation in solution to be suppressed, resulting in reduced antimicrobial effects. Furthermore, prolonged illumination will ultimately lead to reduced integrity of the surface coating, which will result in reduced affinity to bacterial membranes. While these effects are likely to occur also for the presently investigated systems, as seen from the decrease in the ζ-potential upon UV exposure, they are not sufficient to undo the

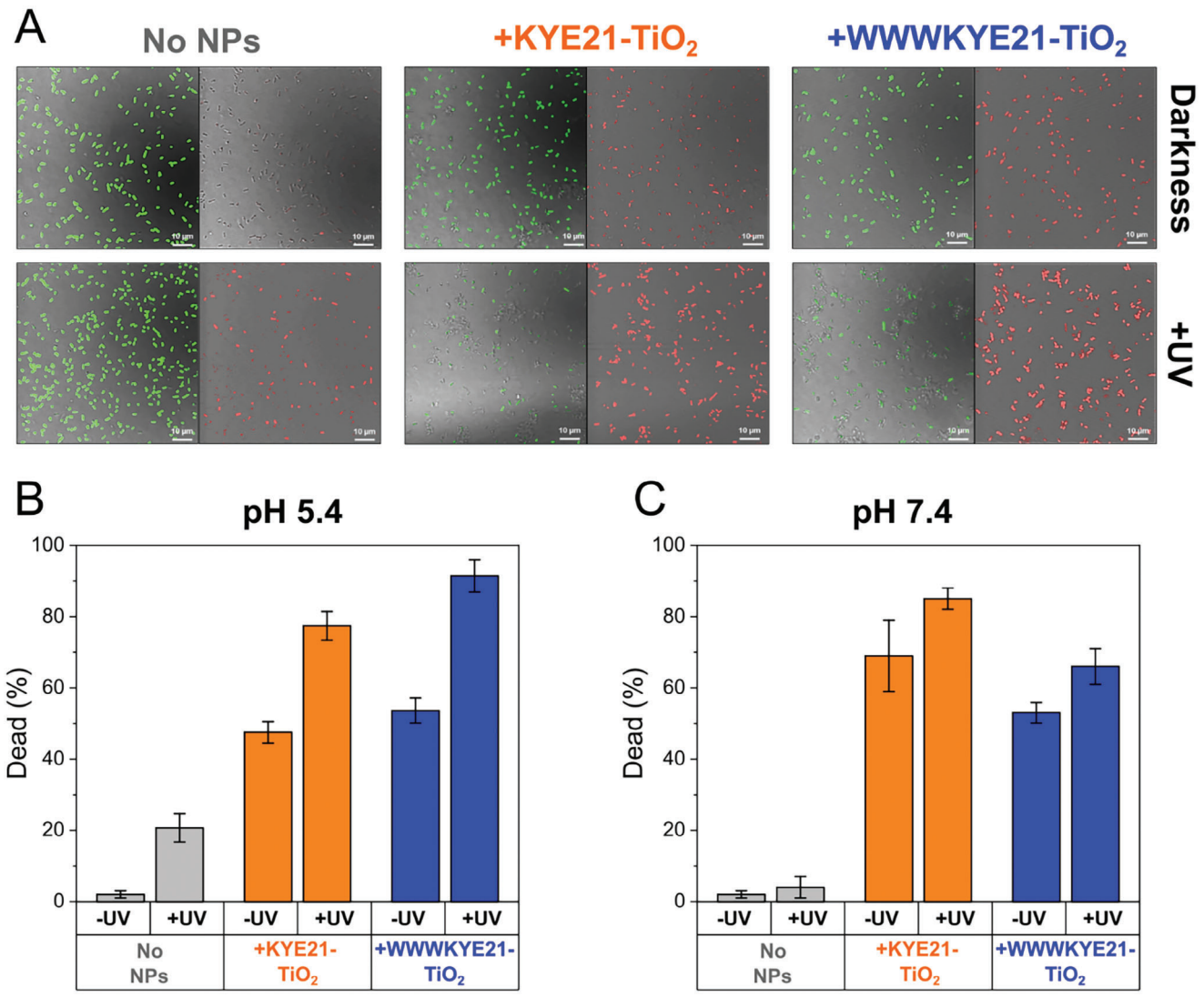

Figure 7. Confocal microscopy results for KYE21- or WWWKYE21-coated TiO_2 NPs interacting with *E. coli* bacteria. A) Representative confocal microscopy images were obtained using LIVE/DEAD assay (red, green, and Differential Interference Contrast images overlaid) for 10^8CFU mL^{-1} of *E. coli* bacteria in 10 mM acetate, pH 5.4, without or with 1 h of incubation with KYE21-coated or WWWKYE21-coatedTiO_2 NPs with or without in situ UV illumination. For each system, live (green) and dead (red) bacteria are shown in separate images (left images for alive bacteria and right images for dead ones). Corresponding images in 10 mM Tris, pH 7.4, are reported in Figure S19 (Supporting Information). (B and C) Quantification of confocal microscopy images, showing percentages of dead *E. coli* bacteria with (+UV) or without (−UV) UV illumination. Results are shown for bacteria alone and for bacteria exposed for 1 h to KYE21-TiO_2 or WWWKYE21-TiO_2 NPs, in (B) 10 mM acetate, pH 5.4, and C) 10 mM Tris, pH 7.4, with or without UV illumination. ($n = 3$).

positive effects of the peptide coating on nanoparticle binding to bacteria-like lipid membranes and LPS over relevant timescales. The absence of any substantial effects of the peptide coatings on ROS generation suggests that the adsorbed peptide layers contain relatively high amounts of water, consistent with previous findings of adsorbed polypeptide and protein layers.[41–44] The results are also in line with previous findings by Caselli et al., showing LL-37 coatings on TiO_2 nanoparticles to be able to endure UV exposure for at least 2 h without losing their net positive charge and their ability to strongly promote binding of LL-37-coated TiO_2 to bacteria-like lipid membranes.[7]

3.2. Membrane Interactions of AMP-Coated NPs

As a result of promoted binding to anionic bacteria membranes, cationic nanoparticles display higher antimicrobial effects than uncharged and negatively charged ones,[38] unless they are sufficiently cationic to trigger extensive binding of anionic serum components, resulting in a negatively charged nanoparticle corona.[45] For most cationic surface modifications, however, boosted antimicrobial effects come at the price of increased toxicity.[45–47] Considering this, AMP coating represents an attractive approach for nanoparticle surface modifications, since such peptides can be designed to display potent antimicrobial

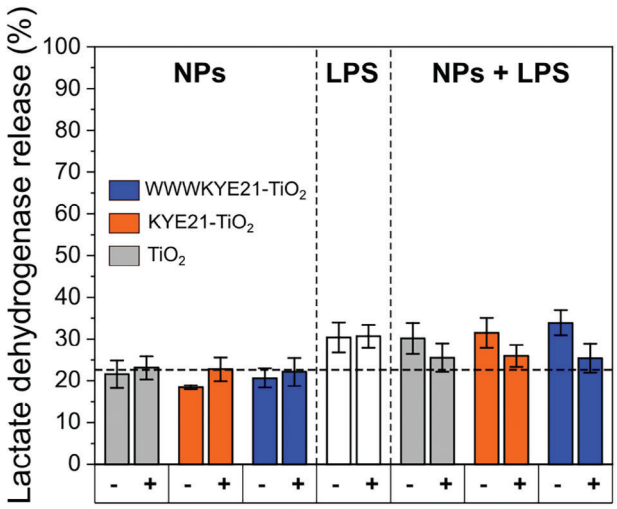

Figure 8. LDH release induced by smooth LPS, in the absence and in the presence of bare, KYE21-coated, or WWWKYE21-coated TiO_2 NPs, either before (−) or after (+) 2 h of UV illumination, using THP1-XBlue-CD14 reporter monocytes in 10 Mm Tris, pH 7.4. The dashed line represents the background release in buffer. ($n = 3$).

effects but simultaneously low cell toxicity.[8,9] Here, the focus was placed on KYE21 and WWWKYE21, for which previous studies have demonstrated the W-tag to strongly boost antimicrobial effects.[13] The pronounced affinity for bacteria displayed by WWWKYE21 comes from the W-residues strongly binding to, and inserting into anionic and cholesterol-void bacterial membranes. As W moieties are bulky and polar enough to reside in the headgroup of the membrane lipids,[48–50] peptide anchoring requires area expansion of the membranes. In the presence of cholesterol, which increases the expansion modulus of mammalian cell membranes,[19] this thus comes at a cost of energy. Particularly in the simultaneous absence of anionic phospholipids, this strongly suppresses the binding, insertion, and destabilization of mammalian cell membranes for the free peptide. For WWWKYE21 attached to TiO_2 nanoparticles, however, the situation is different than for the free peptide since i) the peptide molecules are bound to the nanoparticle surface and hence not free to insert into the lipid membrane, and ii) solvency conditions dictate that the hydrophobic W-residues are likely either bound to the nanoparticle surface or located in the inner region of the adsorbed peptide layer. Analogously, the charged KYE21 moiety may be bound in an orientation that maximizes proximity between the cationic residues and the anionic TiO_2 surface, thereby resulting in an effective lowered positive charge density of the outer peptide layer. As shown in the present study, however, both KYE21-TiO_2 and WWWKYE21-TiO_2 displayed extensive binding to anionic and cholesterol-void +PG bilayers, whereas lower binding was observed for zwitterionic PC and +Chol bilayers, showing at least some of the favorable effects provided by the W-tag and the net positive charge to be retained after NP binding.

3.3. Oxidative Destabilization by AMP-Coated NPs

Upon illumination, +PG bilayers correspondingly displayed the largest susceptibility to oxidative destabilization, in line with previous findings by Caselli et al. for LL-37-coated TiO_2 nanoparticles.[7] At first sight, this may be taken as only a consequence of the higher amount of peptide-coated nanoparticles bound to such membranes than to zwitterionic PC and +Chol. It should be kept in mind, however, that the presence of charged headgroups in anionic phospholipid membranes generally results in less dense packing than for zwitterionic ones.[32,33] It is therefore possible that the degree of particle insertion differs between the systems investigated.[51,52] It has also been suggested that anionic phospholipids display another mechanism for oxidative degradation than zwitterionic ones.[53,54] All of these effects likely contribute to the higher susceptibility to oxidative degradation observed for +PG bilayers.

3.4. Limits of the Analogy Between Free AMPs and AMP-Coated NPs

To shed further light on the effect of the number of nanoparticles bound on their ability to trigger oxidative degradation on UV illumination, the concentration dependence of nanoparticle binding and UV-induced membrane destabilization was investigated for +PG bilayers (Figure S20, Supporting Information). From such experiments, it was found that the binding of both KYE21-TiO_2 and WWWKYE21-TiO_2 increased with particle concentration. Furthermore, UV-induced membrane destabilization showed the highest concentration dependence at low particle concentrations, and gradual saturation at higher particle concentrations (**Figure 9A**). The latter is likely due to the diffuse scattering of membrane-bound nanoparticles, effectively deflecting some of the light and resulting in less efficient ROS generation per particle[55,56] at higher particle concentrations. Such effects have been previously observed for both photocatalytic inactivation of bacteria,[57,58] and for photocatalytic degradation of organic toxins.[59] Considering this concentration dependence, saturation effects are likely responsible for the observation that while the binding of WWWKYE21 to +PG bilayers was much higher than that of KYE21, oxidative degradation caused by WWWKYE21 was only modestly larger than that for KYE21. Hence, the favorable effects of the W-tags,[60,61] are moderated by saturation in oxidative capacity at high nanoparticle binding densities. As shown in Figures 9B and S21 (Supporting Information), similar effects were seen for LPS.

3.5. Bacteria and Cell Interactions of AMP-Coated NPs

Mirroring the results for the LPS and bacteria-like +PG model systems, photocatalytic lysis of *E. coli* bacteria was comparable for WWWKYE21-TiO_2 and KYE21-TiO_2 (Figure 7). Finally, we note that bacteria retained their overall structure on photocatalytic exposure, instead of losing integrity through the formation of local defects. This is an important finding since NP- and/or UV-induced formation of bacterial fragments could potentially deteriorate bacterial infections. The absence of such effects is in line with observations in the literature of efficient inactivation of LPS and bacteria after photocatalytic degradation.[62–66] Together, these results (summarized in **Figure 10**) indicate photocatalytic degradation represents a promising approach for combatting

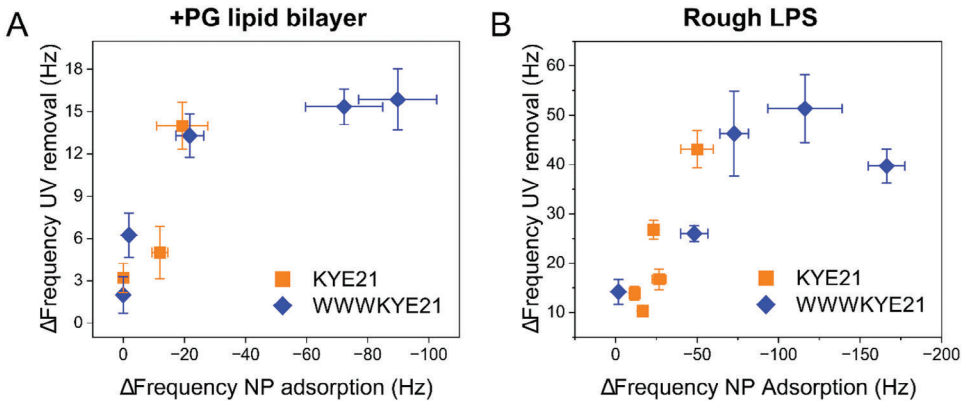

Figure 9. QCM-d results show the dependence of oxidative degradation of +PG A) and rough LPS B) on the amount of NPs bound prior to UV illumination (frequency shift determined by QCM-d) for NP concentrations below the bilayer destabilization threshold. $\Delta F = 0$ and $\Delta D = 0$ correspond to Frequency and Dissipation shifts for +PG and rough LPS right before NP binding. Corresponding results on binding and oxidation as a function of NP concentration, as well as representative QCM-d binding kinetics showing bilayer destabilization threshold, are reported in Figure S20 (Supporting Information) (for +PG) and Figure S21 (Supporting Information) (for rough LPS). Measurements were performed in 10 mM Tris, pH 7.4. ($n = 3$).

bacterial infections, which can be boosted by AMP coating. Here, W-tagging offers functional advantages related to improved colloidal stability as well as enhanced binding affinity to bacterial membranes, which may be valuable for co-aggregation with bacteria and LPS for the confinement of bacterial infections.[67] Having said that, the present study also identifies limitations in the analogy between free and surface-bound AMPs, related to: i) charged and hydrophobic AMP residues being partially "consumed" on nanoparticle binding and thus not being fully available for bacterial membrane interactions, and ii) saturation of photocatalytic effects at high nanoparticle densities in bacterial membranes.

3.6. Input From Related Research Areas

Finally, we note that membrane interactions for other types of NPs may be of relevance for photocatalytic NPs.[1–4] Examples of this include, e.g., work done on light-responsive AuNPs regarding the dynamics and exchange of capping ligands for such systems and how these influence membrane interactions and antimicrobial effects.[68–71] Furthermore, NP interactions with membrane domains[72,73] may potentially be important also for photocatalytic NPs. These aspects represent future research extensions for photocatalytic NPs.

4. Conclusion

Both KYE21 and WWWKYE21 bind to TiO_2 nanoparticles, rendering these positively charged and well-dispersed at physiological pH. The peptide coatings do not substantially suppress ROS formation upon UV illumination and are sufficiently resilient to allow improved nanoparticle binding to bacterial-like lipid membranes and LPS. In consequence, the peptide-coated TiO_2 nanoparticles potently degrade bacteria-like +PG bilayers, as well as LPS. While W-tagging strongly promotes the binding of the peptide-coated nanoparticles to bacteria-like membranes and LPS alike, oxidative degradation reaches saturation at high particle binding, likely related to light scattering. As a result of this, the effects of W-tagging were more modest for oxidative degradation than for nanoparticle binding. Neutron reflectometry results showed that binding of peptide-coated nanoparticles to bacteria-like lipid membranes resulted in partial membrane destabilization in the absence of UV and that UV illumination caused additional increases in the area per molecule, as well as in the hydration of both headgroup and acyl chain regions of the membrane. For smooth LPS, UV-illumination caused the removal of its outer O-antigen region. Finally, peptide-coated nanoparticles displayed potent antimicrobial effects against *E. coli* bacteria, which were further enhanced on UV exposure. In contrast, toxicity against human monocytes remained low after peptide coating. In relation to previous literature,[7] the ms demonstrates that several key aspects of AMPs in solution are translated to AMP-coated photocatalytic nanoparticles, including effects of peptide amphiphilicity on its affinity for bacterial lipids and lipopolysaccharides, as well the selectivity between bacteria and cell membranes provided by W-tagged AMPs. This analogy between free AMP and AMP-coated nanoparticles is a result of likely importance since it means that knowledge obtained on AMPs in solution in previous literature can be used when designing AMP-coated nanoparticles for potency and selectivity. The study also demonstrates a limit of the analogy between free AMPs and AMP-coated photocatalytic nanoparticles at very high particle binding to bacteria membranes and lipopolysaccharides due to light scattering effects limiting photocatalytic degradation.

5. Experimental Section

Materials: TiO_2 NPs (anatase, stated to be 4–8 nm by the manufacturer) were obtained from PlasmaChem GmHb (Berlin, Germany). The nanoparticles were previously characterized by cryoTEM and Small-Angle X-ray scattering (SAXS) to evaluate their size distribution.[7] To obtain reliable information on the primary particle size (i.e., not affected by aggregation), measurements were performed at pH 3.4, where TiO_2 NPs are well dispersed. While SAXS results fitted to a lognormal distribution yielded an average nanoparticle size of 3 ± 1 nm, cryo-TEM results showed the occurrence of polydisperse particles with an average diameter of 2 ± 1 nm, but sizes ranging between 0 and 10 nm. The peptides KYE21 (KYEITTIHNLFRKLTHRLFRR) and WWWKYE21 (>95%) were from Thermo Fisher

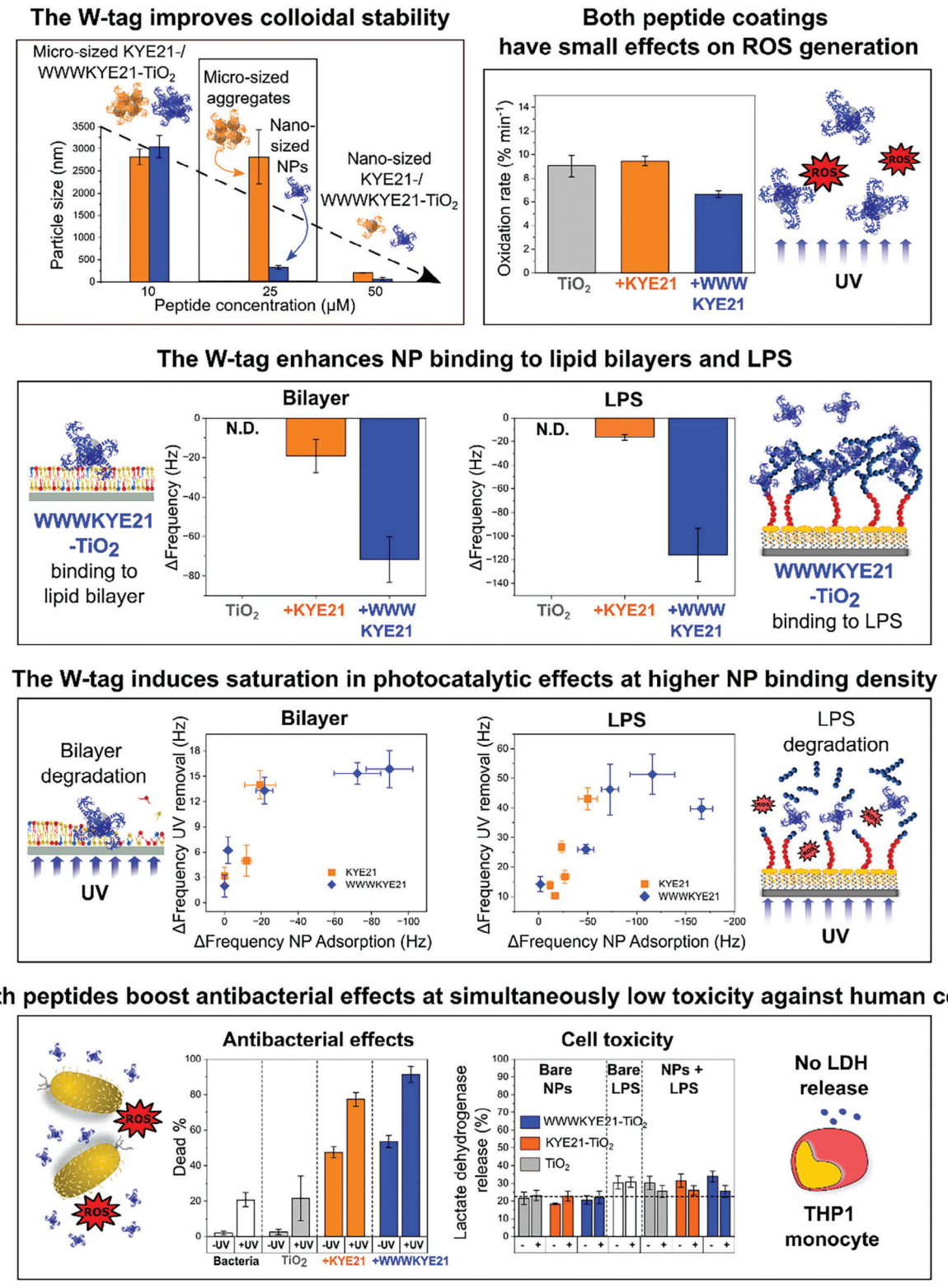

Figure 10. Schematic illustration summarizing the effects of the W-tag moiety on membrane interactions and antimicrobial effects of peptide-coated TiO_2 NPs: Coating TiO_2 NPs by positively charged peptides improves their colloidal stability, especially for WWWKYE21-TiO_2 NPs, while not detrimentally interfering with ROS generation. In addition, the peptide coating significantly enhances TiO_2 binding to bacteria-mimicking +PG bilayers and LPS, particularly so for the W-tagged peptide. As a result of this, WWWKYE21-TiO_2 NPs boosted oxidative degradation of +PG bilayers and LPS upon UV illumination, with saturation of photocatalytic effects observed at high NPs binding density. Mirroring this, peptide-coated TiO_2 NPs displayed boosted antimicrobial effects against Gram-negative *E. coli*, whereas toxicity against human THP1 monocytes remained low.

Scientific (US). Palmitoyloleoylphosphocholine (POPC), palmitoylarachidonoyl phosphocholine (PAPC), palmitoyloleoylphosphoglycerol) (POPG), and cholesterol (bovine, Chol) (all >99% purity) were from Avanti Polar Lipids (Alabaster, US), while C_{11}-BODIPY 581/591 was from Molecular Probes/Thermo Fisher Scientific (US). Tris buffer (Trizma base, ≥99.9%), sodium chloride (≥99.0%), calcium chloride dihydrate (≥99.0%), anhydrous toluene (≥99.0%), and trichloro(octadecyl)silane (OTS, ≥90.0%) were from Sigma Aldrich. Similarly, smooth LPS from *E. coli* O111:B4 (L2630), rough LPS from *E. coli* F583 (Rd mutant) (L6893), and diphosphoryl lipid A from *E. coli* F583 (Rd mutant) (L5399) were from Sigma Aldrich. MilliQ water (MQ, 18.2 MΩ cm^{-1}) and D_2O (99% deuterated, Sigma Aldrich) were used throughout. All other chemicals were of analytical grade.

Liposome Preparation: Liposomes were prepared as described previously.[74] In short, 10 mg mL^{-1} lipid stocks in chloroform (POPC and PAPC) or chloroform/methanol (3/1 vol%) (POPG) were prepared in dark glass vials to (75/25 mol% POPC/PAPC) ("PC"), (50/25/25 mol% POPC/PAPC/POPG ("+PG"), or 65/25/10 mol% POPC/PAPC/Chol ("+Chol"), or to corresponding systems with PAPC replaced by POPC. The lipids were dried under N_2 and then under vacuum. The resulting films were hydrated with either MQ (to form supported lipid bilayers), 10 mM Tris, pH 7.4, or acetate buffer, pH 5.4 (for ROS studies). The resulting multilamellar vesicles were tip sonicated (UP50H, Hielscher Ultrasonics GmbH, Germany (50 W, 30 kHz) used in an intermittent-pulse mode (5 s), at 100% amplitude) for 15 min in an ice bath to obtain ≈30 nm small unilamellar vesicles (SUV; for supported bilayers), or extruded 30 times through polycarbonate filters (Ø 100 nm, LipoFast mini extruder (Avestin, Ottawa, Canada)) to obtain large unilamellar vesicles (LUV; for ROS studies).

Size and ζ-Potential Measurements: Dynamic and electrophoretic light scattering (DLS and ELS; 173° back-scattering angle) was performed using a Zetasizer Nano ZSP (Malvern Pananalytical Ltd., Malvern, UK) to obtain particle size and ζ-potential characteristics. Measurements were performed in triplicates at 25 °C using automatic attenuation and were reported as number-average effective particle diameters.

C_{11}-BODIPY 581/591 Oxidation Assay: ROS generation was investigated as described previously.[74] C_{11}-BODIPY 581/591 was incorporated into PC, +Chol, and +PG bilayers by adding 0.5 mol% of the probe prior to lipid film drying, keeping it under Ar atmosphere. After vesicle formation, LUVs were illuminated by UV (Spectroline ENF-260C, 254 nm; 3 mW cm^{-2}, sample-lamp distance ≈6 cm) in the presence or absence of peptide-coated TiO_2 nanoparticles. Fluorescence spectra (λ_{ex} = 485 nm; λ_{em} = 500–700 nm) were acquired using a Cary Eclipse fluorescence spectrophotometer with Xe pulse lamp (Agilent Technologies, USA). Oxidation was quantified from the spectral shift of the probe emission. All measurements were performed in duplicate at 37 °C.

Quartz Crystal Microbalance with Dissipation Monitoring (QCM-d): QCM-d measurements were performed using a QSense Analyzer with both standard and UV-transparent sapphire window modules (Biolin Scientific, Sweden). Cells and tubing were cleaned with a 2% Hellmanex and then by MQ rinsing under bath sonication, followed by rinsing in ethanol and N_2 drying. SiO_2 surfaces (QSense QSX 303 SiO_2, 4.95 ± 0.05 MHz) were washed in Hellmanex 2%/MQ/ethanol, dried with N_2, and plasma cleaned (Model PDC-32G, Harrick Plasma, USA). A liquid flow of 0.1 mL min^{-1} was employed throughout the experiments. For experiments with lipid bilayers, SiO_2 surfaces were mounted in the measurement cells without further modification. PC, +Chol, and +PG bilayers were prepared by SUV deposition on SiO_2 surfaces as described previously.[74] Briefly, SUVs (0.1 mg mL^{-1} in MQ) were injected using a peristaltic pump, followed by MQ rinsing to remove nonadsorbed vesicles. Full vesicle rupture and bilayer formation were confirmed by changes in frequency (ΔF) of −23 ± 1 Hz and dissipation (ΔD) of (0.25 ± 0.25)·10^{-6}. This was followed by rinsing with buffer (10 mM Tris, pH 7.4, or acetate, pH 5.4) and the addition of either bare or peptide-coated TiO_2 nanoparticles. Subsequently, the buffer was flushed for 10 min to remove NP excess. Finally, samples were illuminated by UV light (Spectroline lamp ENF-260C, 6 W, 254 nm; 3 mW cm^{-2}, placed at ≈2 cm from the QCM-d cell) for 2 h, followed by buffer rinsing. Measurements were performed at 25 °C in triplicates. For experiments with LPS and lipid A, SiO_2 surfaces were dried at 70 °C for 10 min immediately after plasma cleaning and then transferred to a toluene solution containing OTS (1 mM).[34,35] After 1 h, they were rinsed with toluene and ethanol, dried under N_2, and mounted into the measurement cell. After that, 10 mM Tris buffer containing 150 mM NaCl and 4 mM $CaCl_2$ was flushed into the cell (10 min), followed by rinsing with the same buffer without $CaCl_2$ (10 min). Subsequently, solutions of LPS (1000 ppm) in 150 mM NaCl, 10 Mm Tris were injected, right after tip-sonication for 10 min (UP50H, Hielscher Ultrasonics GmbH, Germany (50 W, 30 kHz) used in an intermittent-pulse mode (5 s), at 100% amplitude) and allowed to deposit for 30 min. Excess LPS was rinsed off by buffer flushing for 10 min. Then, NPs were added, and UV illumination was applied using the same protocol as for lipid bilayers. Measurements were performed at 25 °C in triplicates.

Neutron reflectometry (NR): NR experiments on supported +PG bilayers interacting with WWWKYE21-coated TiO_2 NPs and smooth LPS interacting with bare or WWWKYE21-coated TiO_2 NPs were performed on the OffSpec reflectometer (ISIS Pulsed Neutron and Muon Source, Rutherford Appleton Laboratory, Harwell, UK[75]). Three incident angles (0.3°, 1.0° and 2.3°) were used to cover the Q-region from ≈0.01 to 0.35 $Å^{-1}$, with an instrumental resolution of 0.04 (4%) dq/q. Solid-liquid flow cells with the top plate modified with a 30 mm diameter opening, were used together with UV-transparent quartz blocks (80 × 50 × 15 mm, 1 face polished, RMS <4.5 Å, PI-KEM Ltd., Tamworth, UK) to allow in situ UV irradiation. HPLC tubing, PEEK troughs, and O-rings were cleaned with 2% Hellmanex (Hellma Analytics, UK) under sonication, then thoroughly rinsed and sonicated in MQ. Cells were connected to a circulating water bath during the measurements to keep them at 25 °C. For experiments on +PG bilayers, the blocks were cleaned in piranha solution (5/4/1 $H_2O/H_2SO_4/H_2O_2$) at 80 °C for 15 min (*Caution: Piranha solution is highly corrosive*), rinsed thoroughly in MQ, followed by 10 min of UV-ozone treatment (UV/Ozone ProCleaner, BioForce Nanosciences, USA). After that, blocks were mounted in the solid-liquid flow cells and characterized in D_2O and MQ H_2O. Then, tip-sonicated SUV suspensions (0.1 mg mL^{-1}) were injected manually and allowed to deposit for 20 min, after which the excess was rinsed off with 10 mL MQ and 10 mL of 10 mM Tris buffer, pH 7.4, at 2 mL min^{-1}. The bilayers thus formed were characterized in three contrasts; d-, qm- and h-buffer, i.e., 10 mM Tris buffer in D_2O, 68.6/31.4% v/v D_2O/H_2O mixture (with scattering length density (SLD) matching the one of quartz), and H_2O, respectively) before treatment. Contrasts were exchanged by pumping 20 mL of the desired buffer at 2 mL min^{-1}. Subsequently, peptide-coated TiO_2 nanoparticles (20 ppm) in h-buffer were injected manually and incubated for 10 min with the bilayer. H-buffer was subsequently flushed to remove the excess of NPs and the reflectivity was acquired in the three contrasts. The bilayers were then subjected to in situ UV irradiation (Spectroline lamp ENF-260C, 6 W, 254 nm; 3 mW cm^{-2}) for 2 h, placed at ≈2 cm from the NR cell. After UV exposure, the whole Q range was measured in d-, qm-, and h-buffers. For experiments with supported LPS, the quartz blocks were cleaned by bath-sonication for 30 min in chloroform, followed by acetone (30 min), ethanol (30 min), MQ H_2O (30 min), and ethanol (30 min) again. Subsequently, they were dried under N_2, followed by 30 min of UV-ozone treatment (UV/Ozone ProCleaner, BioForce Nanosciences, USA). After that, they were dried in an oven (100 °C) for 10 min and transferred to a solution of anhydrous toluene containing OTS (1 mM), and incubated for 1 h in a glovebox under nitrogen flow.[34,35] Blocks were finally rinsed with toluene and ethanol, dried under N_2 and mounted in solid-liquid flow cells. OTS-coated surfaces were first characterized in h-, qm-, and d-buffers (10 mM Tris, 150 mM NaCl, pH 7.4). Then, they were rinsed with an h-buffer containing $CaCl_2$ 4 mM (10 min, 2 mL min^{-1}), followed by rinsing with an h-buffer (10 min, 2 mL min^{-1}). Twenty mL of LPS dispersions in an h-buffer (1000 ppm) were then injected manually, right after tip-sonication (10 min, UP50H, Hielscher Ultrasonics GmbH, Germany), and allowed to deposit for 30 min, after which the excess was rinsed off with 10 mL h-buffer at 1 mL min^{-1}. The layers thus formed were characterized in h-, qm-, and d-buffers, exchanged by pumping 20 mL of each buffer at 1 mL min^{-1}. After that, either 15 mL of bare or peptide-coated TiO_2 NPs in h-buffer (100 and 20 ppm, respectively) were injected, followed by 10 min of incubation. H-buffer was

subsequently flushed to remove the excess of NPs and the samples were characterized in the three contrasts. The systems were then subjected to in situ UV irradiation for 2 h, after which the whole Q range was measured in the three contrasts. The reflected intensity was measured as a function of the momentum transfer $q_z = (4\pi\backslash\lambda)\cdot\sin(\vartheta)$, where λ is wavelength and ϑ is the incident angle. By fitting the experimental data, quantitative information about the density profile of the sample normal to the interface can be obtained. Experimental NR profiles were fitted by using the Genetic Optimization method available on the Motofit analysis package within the software IGOR Pro.[76,77] A series of parallel layers were used to model the interfacial structure, each of these described by thickness, roughness, hydration, and SLD. Monte Carlo error analysis allowing for refitting data 200 times was employed to minimize the uncertainty associated with data fitting.[78]

LIVE/DEAD Bacterial Viability Assay: *E. coli* ATCC 25922 were stained using the LIVE/DEAD BacLight Bacterial Viability Kit (Thermo Fisher Scientific Inc., Waltham, USA). Bacteria were grown to stationary phase in 25 mL Lennox broth (LB Broth; Sigma Aldrich (St. Luis, USA)) overnight at room temperature under shaking at 180 rpm. The bacteria were pelleted and washed by centrifugation (10 000 × g, 10 min, twice) and resuspended either in 10 mM Tris, pH 7.4, or in 10 mM acetate, pH 5.4. Nanoparticle dispersions (500 µL), either bare or loaded with either KYE21 or WWWKYE21, were added to 500 µL of bacteria suspensions. In the final mixture, NPs had a concentration of 100 ppm, while the optical density OD600 of the dispersion was 1.2, corresponding to 12×10^8 *E. coli* colony forming units (CFU)/mL (confirmed on subsequent dilution, plating, culture, and counting of colonies). Samples were then placed in quartz cuvettes and incubated for 1 h at room temperature, either in darkness or under UV illumination (Spectroline ENF-260C, 254 nm; 3 mW cm^{-2}), the latter at a cuvette-lamp distance of 6 cm. Samples were subsequently diluted in the buffer to obtain an OD600 of 0.6, corresponding to 6×10^8 CFU/mL *E. coli*. This was followed by 10 min staining of 200 µL of the sample with 0.5 µL of a 1/1 (v/v) mixture of the fluorescent probes SYTO 9 (excitation/emission maxima 480/500 nm) and propidium iodide (excitation/emission maxima 490/635 nm).[79] Subsequently, samples were imaged by confocal microscopy. Bacteria were plated onto a cover slide at 10^8 CFU mL^{-1} and then imaged with a 100×/1.25 oil objective using a Leica DMi8 confocal microscope (Leica Microsystems, Washington, D.C., USA). For each sample, 20 randomized, wide-field images (100 µm × 100 µm) were collected. Quantification of the fraction of LIVE/DEAD bacteria was performed with the software ImageJ (National Institutes of Health, Bethesda, USA).[80,81] Experiments were run in triplicates at 25 °C.

Lactate Dehydrogenase (LDH) Assay: To investigate cell toxicity, human monocytes (THP1-Xblue-CD14 reporter cells (InvivoGen, France)) were cultured according to the manufacturer's instructions, and nanoparticle-induced release of the intracellular enzyme LDH was monitored. For this, bare or peptide-coated TiO_2 NPs (100 ppm) were mixed with 10 ppm LPS in 10 mM Tris, pH 7.4. Samples were then placed in quartz cuvettes and incubated for 2 h at room temperature, either in darkness or under UV illumination (Spectroline ENF-260C, 254 nm; 3 mW cm^{-2}), at a cuvette-lamp distance of 6 cm. Corresponding controls, containing bare or peptide-coated TiO_2 NPs only, as well as LPS only, were similarly prepared. Then, samples were incubated with cells (1×10^6 cells mL^{-1}). To be able to compare results for cells and bacteria, LDH experiments were performed at an average of 250 TiO_2 NPs per cell, which is comparable to that used for confocal microscopy studies of bacteria (≈200 nanoparticles per CFU). After 22–24 h incubation at 37 °C in 5% CO_2, LDH release was measured in triplicates using a lactate dehydrogenase assay kit (Invitrogen CyQUANT LDH Cytotoxicity Assay, Fisher Scientific), according to manufacturer's instructions.

Statistical Analysis: All data are reported as means with related standard errors. For every experiment described in this work (except for neutron reflectometry), measurements were performed in at least triplicate. For neutron reflectometry, errors associated with the structural parameters of the lipid bilayers or lipopolysaccharides layers were obtained through a Monte Carlo error analysis,[78] available on the Motofit software within the IGOR Pro analysis package.[76,77] This enabled the refit of experimental neutron reflectometry profiles 200 times, minimizing the uncertainty associated with data fitting.

Supporting Information

Supporting Information is available from the Wiley Online Library or from the author.

Acknowledgements

The authors thank ISIS (10.5286/ISIS.E.RB2310291) for access to neutron beam time. The research was funded by the Swedish Research Council (Grant number 2021–05498; L.C., M.M.), Independent Research Fund Denmark (Grant number 9040-00020B; L.C., M.M.), as well as the LEO Foundation Center for Cutaneous Drug Delivery (Grant number LF15007; M.M.). The neutron beamtime was awarded by ISIS (10.5286/ISIS.E.RB2310291).

Conflict of Interest

The authors declare no conflict of interest.

Author Contributions

C.L.C. and T.T. contributed equally to this work. L.C. and M.M. designed the study and wrote the paper, which was reviewed by all authors. All authors were involved in performing the experiments and the interpretation of experimental results.

Data Availability Statement

The data that support the findings of this study are available in the supplementary material of this article.

Keywords

antimicrobial peptide, membrane, nanoparticle, photocatalysis, TiO_2, tryptophan

Received: March 23, 2024
Revised: June 13, 2024
Published online: June 20, 2024

[1] E. Parra-Ortiz, M. Malmsten, *Adv. Colloid Interface Sci.* **2021**, *299*, 102526.
[2] A. Gupta, S. Mumtaz, C.-H. Li, I. Hussain, V. Rotello, *Chem. Soc. Rev.* **2019**, *48*, 415.
[3] N.-Y. Lee, W.-C. Ko, P.-H. Hsueh, *Front. Pharmacol.* **2019**, *10*, 1153.
[4] M. Xie, M. Gao, Y. Yun, M. Malmsten, M. V. Rotello, R. Zboril, O. Akhavan, A. Kraskouski, J. Amalraj, R. Fakhrullin, X. Cai, J. Lu, H. Zheng, R. Li, *Angew. Chem., Int. Ed.* **2023**, *62*, 202217345.
[5] A. Sułek, B. Pucelik, J. Kuncewicz, G. Dubin, J. M. Dabrowski, *Catal. Today* **2019**, *335*, 538.
[6] F. Y. Ahmed, U. F. Aly, R. M. Abd El-Baky, N. G. F. M. Waly, *Int. J. Nanomed.* **2020**, *15*, 3393.
[7] L. Caselli, E. Parra-Ortiz, S. Micciulla, M. W. A. Skoda, S. M. Häffner, E. M. Nielsen, M. J. A. van der Plas, M. Malmsten, *Small* **2024**, 2309496.

[8] T. Rončević, J. Puizina, A. Tossi, *Int. J. Mol. Sci.* **2019**, *20*, 2713.
[9] M. Pasupuleti, A. Schmidtchen, M. Malmsten, *Crit. Rev. Biotechnol.* **2012**, *32*, 143.
[10] R. E. W. Hancock, E. F. Haney, E. E. Gill, *Nat. Rev. Immunol.* **2016**, *16*, 321.
[11] A. Schmidtchen, M. Malmsten, *Curr. Opin. Colloid Interface Sci.* **2013**, *18*, 381.
[12] L. Martin, A. van Meegern, S. Doemming, T. Schuerholz, *Front. Immunol.* **2015**, *6*, 404.
[13] S. Singh, A. Datta, A. Bhunia, M. Malmsten, *Sci. Rep.* **2017**, *7*, 212.
[14] R. Allsopp, A. Pavlova, T. Cline, A. M. Salyapongse, R. E. Gillian, Y. P. Di, B. Deslouches, J. B. Klauda, J. C. Gumbart, S. Tristram-Nagle, *J. Phys. Chem. B* **2022**, *126*, 6922.
[15] T. L. Santos, A. Morales, C. R. Nakaie, F. C. L. Almeida, S. Schreier, A. P. Valenta, *Biophys. J.* **2016**, *111*, 2676.
[16] C. W. Haest, J. de Gier, J. A. den Kamp, P. Bartels, L. L. van Deenen, *Biochim. Biophys. Acta* **1972**, *255*, 720.
[17] R. F. Epand, P. B. Savage, R. M. Epand, *Biochim. Biophys. Acta* **2007**, *1768*, 2500.
[18] G. van Meer, *Ann. Rev. Cell Biol.* **1989**, *5*, 247.
[19] J. Henriksen, A. C. Rowat, E. Brief, Y. W. Hsueh, J. L. Thewalt, M. J. Zuckermann, J. H. Ipsen, *Biophys. J.* **2006**, *90*, 1639.
[20] M. Malmsten, G. Kasetty, M. Pasupuleti, J. Alenfall, A. Schmidtchen, *PLoS One* **2011**, *6*, e16400.
[21] A. Schmidtchen, L. Ringstad, G. Kasetty, H. Mizuno, M. W. Rutland, M. Malmsten, *Biochim. Biophys. Acta* **2011**, *1808*, 1081.
[22] K. M. Reddy, S. V. Manorama, A. R. Reddy, *Mater. Chem. Phys.* **2003**, *78*, 239.
[23] E. Proksch, *J. Dermatol.* **2018**, *45*, 1044.
[24] M. Kosmulski, *J. Colloid Interface Sci.* **2006**, *298*, 730.
[25] M. Kosmulski, *Adv. Colloid Interface Sci.* **2002**, *99*, 255.
[26] C. J. Pestana, C. Edwards, R. Prabhu, P. K. J. Robertson, L. A. Lawton, *J. Hazard. Mater.* **2015**, *300*, 347.
[27] M. H. Ahmed, J. A. Byrne, T. E. Keyes, *Mater. Sci. Eng. C.* **2014**, *39*, 227.
[28] S. M. Häffner, E. Parra-Ortiz, M. W. A. Skoda, T. Saerbeck, K. L. Browning, M. Malmsten, *J. Colloid Interface Sci.* **2021**, *584*, 19.
[29] M. Lukacova, I. Barak, J. Kazar, *Clin. Microbiol. Inf.* **2008**, *14*, 200.
[30] F. Di Lorenzo, K. A. Duda, R. Lanzetta, A. Silipo, C. De Castro, A. Molinaro, *Chem. Rev.* **2022**, *122*, 15767.
[31] J. Pan, F. A. Heberle, S. Tristram-Nagle, M. Szymanski, M. Koepfinger, J. Katsaras, N. Kučerka, *Biochim. Biophys. Acta* **2012**, *1818*, 2135.
[32] G. Pabst, S. Danner, S. Karmakar, G. Deutsch, V. A. Raghunathan, *Biophys. J.* **2007**, *93*, 513.
[33] N. Kučerka, F. A. Heberle, J. Pan, J. Katsaras, *Membranes* **2015**, *5*, 454.
[34] N. Paracini, L. A. Clifton, M. W. A. Skoda, J. H. Lakey, *Proc. Natl. Acad. Sci. U.S.A.* **2018**, *115*, E7587.
[35] I. Rodriguez-Loureiro, V. M. Latza, G. Fragneto, E. Schneck, *Biophys. J.* **2018**, *114*, 1624.
[36] S. Micciulla, Y. Gerelli, E. Schneck, *Biophys. J.* **2019**, *116*, 1259.
[37] N. Paracini, E. Schneck, A. Imbery, S. Micciulla, *Adv. Coll. Interface Sci.* **2022**, *301*, 102603.
[38] S. M. Häffner, M. Malmsten, *Adv. Colloid Interf. Sci.* **2017**, *248*, 105.
[39] K. Das, A. Roychoudhury, *Front. Environ. Sci.* **2014**, *2*, 1.
[40] F. Collin, *Int. J. Mol. Sci.* **2019**, *20*, 2407.
[41] D. Forciniti, W. A. Hamilton, *J. Colloid Interface Sci.* **2005**, *285*, 458.
[42] T. J. Su, J. R. Lu, R. K. Thomas, Z. F. Cui, J. Penfold, *Langmuir* **1998**, *14*, 438.
[43] B. M. Manzi, M. Werner, E. P. Ivanova, R. J. Crawford, V. A. Baulin, *Sci. Rep.* **2019**, *9*, 4694.
[44] H. Min, E. Freeman, W. Zhang, C. Ashraf, D. Allara, A. C. T. Van Duin, S. Tadigadapa, *Langmuir* **2017**, *33*, 7215.
[45] N. Duran, C. P. Silveria, M. Duran, D. S. Martinez, *J. Nanobiotechnol.* **2015**, *13*, 55.
[46] K. I. McConnell, S. Shamsudeen, I. M. Meraz, T. S. Mahadevan, A. Ziemys, P. Rees, H. D. Summers, R. E. Serda, *J. Biomed. Nanotechnol.* **2016**, *12*, 154.
[47] M. Weiss, J. Fan, M. Claudel, T. Sonntag, P. Didier, C. Ronzani, L. Lebeau, F. Pons, *J. Nanobiotechnol.* **2021**, *19*, 5.
[48] G. Orädd, A. Schmidtchen, M. Malmsten, *Biochim. Biophys. Acta* **2011**, *1808*, 244.
[49] M. R. R. de Planque, J. A. W. Kreuijtzer, R. M. J. Liskamp, D. Marsh, D. V. K. Greathouse, R. E. Koeppe, B. de Kruijff, J. A. Killian, *J. Biol. Chem.* **1999**, *274*, 20839.
[50] J. L. MacCallum, W. F. D. Bennett, D. P. Tieleman, *Biophys. J.* **2008**, *94*, 3393.
[51] R. Michel, M. Gradzielski, *Int. J. Mol. Sci.* **2012**, *13*, 11610.
[52] G. D. Bothun, N. Ganji, I. A. Khan, A. Xi, C. Bobba, *Langmuir* **2017**, *33*, 353.
[53] W. Y. Tai, Y. C. Yang, H. J. Lin, C. P. Huang, Y. L. Cheng, M. F. Chen, H. L. Yen, I. Liau, *J. Phys. Chem. B* **2010**, *114*, 15642.
[54] E. Schnitzer, I. Pinchuk, D. Lichtenberg, *Eur. Biophys. J.* **2007**, *36*, 499.
[55] P. Calza, M. Minella, L. Demarchis, F. Sordello, C. Minero, *Catal. Today* **2020**, *340*, 12.
[56] A. Tolosana-Moranchel, C. Pecharroman, M. Faraldos, A. Bahamonde, *Chem. Eng. J.* **2021**, *403*, 126186.
[57] A. K. Benabbou, Z. Derriche, C. Felix, P. Lejeune, C. Guillard, *Appl. Catal. B* **2007**, *76*, 257.
[58] M. Karbasi, F. Karimzadeh, K. Raeissi, S. Rtimi, J. Kiwi, S. Giannakis, C. Pulgarin, *Water* **2020**, *12*, 1099.
[59] P. A. Mangrulkar, S. P. Kamble, M. M. Joshi, J. S. Meshram, N. K. Labhsetwar, S. S. Rayalu, *Int. J. Photoenergy* **2012**, *1*, 780562.
[60] K. Yamauchi, Y. Yao, T. Ochiai, M. Sakai, Y. Kubota, G. Yamauchi, *J. Nanotechnol.* **2011**, *1*, 380979.
[61] S. Wooh, N. Encinas, D. Vollmer, H. J. Butt, *Adv. Mater.* **2017**, *29*, 1604637.
[62] J. Kurz, F. Eberle, T. Graumann, M.-E. Kaschler, A. Sähr, F. Neumann, A. H. Dalpke, L. Erdinger, *Chemosphere* **2011**, *84*, 1188.
[63] J. Kiwi, V. Nadtochenko, *Langmuir* **2005**, *21*, 4631.
[64] P. Liu, W. Duan, X. Li, *Coll. Surf. B* **2010**, *78*, 171.
[65] K. Sunada, T. Watanabe, K. Hashimoto, *Environ. Sci. Technol.* **2003**, *37*, 4785.
[66] H. Wu, L. Xie, M. He, R. Zhang, Y. Tian, S. Liu, T. Gong, F. Huo, T. Yang, Q. Zhang, S. Guo, W. Tian, *Acta Biomater.* **2019**, *97*, 597.
[67] S. M. Häffner, L. Nystrom, K. L. Browning, H. M. Nielsen, A. A. Stromstedt, M. J. A. van der Plas, A. Schmidtchen, M. Malmsten, *ACS Appl. Mater. Interf.* **2019**, *11*, 15389.
[68] C. Contini, M. Schneemilch, S. Gaisford, N. Quirke, *J. Exp. Nanosci.* **2018**, *13*, 62.
[69] C. Contini, J. W. Hindley, T. J. Macdonald, J. D. Barritt, O. Ces, N. Quirke, *Com. Chem.* **2020**, *3*, 130.
[70] S. Salassi, L. Caselli, J. Cardellini, E. Lavagna, C. Montis, D. Berti, G. Rossi, *J. Chem. Theory Comput.* **2021**, *17*, 6597.
[71] R. Penman, R. Kariuki, Z. L. Shaw, C. Dekiwadia, A. J. Christofferson, G. Bryant, J. Vongsvivut, S. J. Bryant, A. Elbourne, *J. Colloid Interface Sci.* **2024**, *654*, 390.
[72] R. Kariuki, R. Penman, S. J. Bryant, R. Orrell-Trigg, N. Meftahi, R. J. Crawford, C. F. McConville, G. Bryant, K. Voïtchovsky, C. E. Conn, A. J. Christofferson, A. Elbourne, *ACS Nano* **2022**, *16*, 17179.
[73] A. Ridolfi, L. Caselli, C. Montis, G. Mangiapia, D. Berti, M. Brucale, F. Valle, *J. Microscopy* **2020**, *280*, 194.

[74] E. Parra-Ortiz, S. Malekkhaiat Häffner, T. Saerbeck, M. W. A. Skoda, K. L. Browning, M. Malmsten, *ACS Appl. Mater. Interf. Sci.* **2020**, *12*, 32446.
[75] J. R. P. Webster, S. Langridge, R. M. Dalgliesh, T. R. Charlton, *Eur. Phys. J. Plus.* **2011**, *126*, 112.
[76] A. Nelson, *J. Phys. Conf. Ser.* **2010**, *251*, 012094.
[77] A. Nelson, *J. Appl. Cryst.* **2006**, *39*, 273.
[78] F. Heinrich, T. Ng, D. J. Vanderah, P. Shekar, M. Mihailescu, H. Nanda, M. Lösche, *Langmuir* **2009**, *25*, 4219.
[79] L. Boulos, M. Prevost, B. Barbeau, J. Coallier, R. Desjardins, *J. Microbiol. Methods* **1999**, *37*, 77.
[80] C. A. Schneider, W. S. Rasband, K. W. Eliceiri, *Nat. Methods* **2012**, *9*, 671.
[81] T. J. Collins, *BioTechniques* **2007**, *43*, 25.